CrystEngComm

ROYAL SOCIETY OF CHEMISTRY

PAPER

View Article Online
View Journal | View Issue

Cite this: *CrystEngComm*, 2020, **22**, 3670

Modulating the solubility and pharmacokinetic properties of 5-fluorouracil *via* cocrystallization†

Xia-Lin Dai,[c] Chao Wu,[a] Jin-Hui Li,[d] Lian-Chao Liu,[d] Xin He,[d] Tong-Bu Lu [b] and Jia-Mei Chen *[a]

Received 17th March 2020,
Accepted 22nd April 2020

DOI: 10.1039/d0ce00409j

rsc.li/crystengcomm

5-Fluorouracil (5FU) is a classical anti-metabolic drug with broad-spectrum antitumor effects. However, the oral absorption of 5FU is incomplete with a short biological half-life and an obvious peak-valley phenomenon, leading to the frequent administration requirement and severe side effects. Herein, a pharmaceutical cocrystallization approach based on crystal engineering was employed to modulate the pharmacokinetic properties of 5FU by changing its aqueous solubility. Four cocrystals of 5FU with a group of dihydroxybenzoic acids were synthesized and characterized. The powder dissolution experiments showed that all the cocrystals exhibited different aqueous solubilities and dissolution rates in comparison with pure 5FU. As compared to pure 5FU, the apparent solubility values of two cocrystals were increased by 34% and 11% while those of the other two cocrystals were reduced by 27% and 51%, respectively. The pharmacokinetic parameters of all the cocrystals, including C_{max}, t_{max}, MRT_{0-t}, $t_{1/2}$ and AUC_{0-t}, as well as the shape of the pharmacokinetic curves, were accordingly altered in the *in vivo* pharmacokinetic study. This study has important implications for using cocrystallization techniques to modulate the pharmacokinetic properties of drugs with undesirable oral absorption, especially to avoid the *in vivo* peak-valley effect and reduce side effects in clinical practice.

Introduction

5-Fluorouracil (5FU) is a classical anti-metabolic drug with broad-spectrum antineoplastic effects.[1] It is a pyrimidine analog that can convert into fluorouracil deoxynucleotides to interrupt the synthesis of thymine, and thereby inhibit the synthesis of DNA in tumour cells.[2] In clinic, 5FU is commonly used to treat a variety of cancers including gastrointestinal cancer, breast cancer, ovarian cancer and skin cancer, administered alone or in combination with other drugs.[3–7] However, the oral absorption of 5FU is incomplete and non-uniform in different individuals due to fast metabolism, with a biological half-life of approximately 10–20 min and an obvious peak-valley phenomenon.[8,9] Thus, in order to maintain adequate blood drug concentration, 5FU is usually administered by continuous intravenous drip infusion at a large dosage (typically 15 mg kg^{-1} per day) clinically, which is always accompanied by serious systemic side effects such as myelosuppression, severe mucositis and hematological adverse reactions.[10,11] Oral administration of drugs has the advantages of convenience, good patient compliance and high safety.[12] Therefore, a number of oral delivery systems of 5FU, such as poly(lactide-*co*-glycolide) nanoparticles, poly(lactic acid) or poly(lactic acid)–poly(ethylene glycol) blend nanoparticles and sesbania gum based hydrogel, have been investigated to extend the half-life of 5FU and improve its bioavailability.[13–15] However, these formulations suffer from instability, complex preparation processes and poor reproducibility, which make them difficult to be applied in clinical practice.

Pharmaceutical cocrystals are defined as homogeneous crystalline solids formed by noncovalent bonds, such as hydrogen bonds, π···π and van der Waals interactions, between active pharmaceutical ingredients (APIs) and cocrystal coformers (CCFs).[16] Cocrystals can improve the physicochemical properties of APIs, including solubility, dissolution rate, permeability, and physical and chemical stability as well as mechanical properties, without changing the covalent bonds of the APIs.[17–24] The cocrystallization approach has been extensively used to improve the

[a] *Tianjin Key Laboratory of Drug Targeting and Bioimaging, School of Chemistry and Chemical Engineering, Tianjin University of Technology, Tianjin 300384, China. E-mail: chenjm37@mail.sysu.edu.cn*
[b] *Institute for New Energy Materials and Low Carbon Technologies, School of Materials Science and Engineering, Tianjin University of Technology, Tianjin 300384, China*
[c] *School of Pharmaceutical Sciences, Sun Yat-Sen University, Guangzhou 510006, China*
[d] *College of Veterinary Medicine, Hebei Agricultural University, Baoding 071000, China*

† Electronic supplementary information (ESI) available. CCDC 1970719, 1970721 and 1970722. For ESI and crystallographic data in CIF or other electronic format see DOI: 10.1039/d0ce00409j

bioavailability and druggability of poorly soluble drugs through the increase of the solubility and dissolution rate.[25–29] Recently, several researchers have focused on reducing the solubility and dissolution rate of highly soluble drugs with the intention to slow their *in vivo* absorption and prolong the retention time.[30–33] Compared with the above-mentioned methods, the cocrystallization technique is free from various excipients and complex preparation processes, and is well reproducible on an industrial scale, which has great potential for clinical application.[34,35]

5FU is a soluble drug (about 21 mg mL^{-1} in pH 6.8 phosphate buffer, 37 °C) with poor permeability ($\log P$ = −0.89), which is classified as a class III drug based on the Biopharmaceutics Classification System (BCS).[36,37] To date, studies on the cocrystallization of 5FU with various CCFs including cinnamic acid, 4-aminobenzoic acid, salicylic acid, 3-hydroxybenzoic acid, 4-hydroxybenzoic acid, 4-aminopyridine, 3,4-dihydroxybenzoic acid, gentisic acid, 3-hydroxy-2-naphthoic acid and 6-hydroxy-2-naphthoic acid have been reported and have focused on the *in vitro* permeability for the topical delivery of 5FU.[36,38–40] Moreover, other 5FU cocrystals with 5-fluorocytosine, 4-methylbenzoic acid, 3-nitrobenzoic acid, *trans*-bis(2-pyridyl)ethylene, cytosine, 1-methylcytosine, theophylline, urea, thiourea, 2,2′-bipyridine, 4,4′-bipyridine, acridine, phenazine, 4,4-bispyridylethene, adenosine, *etc.* have also been reported.[41–49]

However, no cocrystals of 5FU have been reported concerning *in vivo* pharmacokinetic properties following oral administration. In order to modulate the solubility and dissolution rate of 5FU and thereby ameliorate its pharmacokinetic properties, four cocrystals with a group of dihydroxybenzoic acids, namely 3,4-dihydroxybenzoic acid (34DHBA), 3,5-dihydroxybenzoic acid (35DHBA) and 2,5-dihydroxybenzoic acid (25DHBA), were prepared in this paper, including three anhydrous cocrystals (**5FU–34DHBA**, **5FU–35DHBA** and **5FU–25DHBA**) and one hydrate form (**5FU–34DHBA·2H$_2$O**) (Scheme 1). 34DHBA, 35DHBA and 25DHBA are naturally occurring phenolic acids with various pharmacological activities. 34DHBA has been found to have antioxidant, anticancer, anti-inflammatory, antibacterial, antidiabetic, antiaging, and antiviral effects, *etc.*[50] 35DHBA shows hydrogen peroxide scavenging, antioxidant and anti-radical activities.[51] 25DHBA is a natural product from the root of the genus *Gentiana* with biological activities such as antitumor, anti-mutagenicity, anti-inflammatory, antioxidant, hepatoprotective and neuroprotective activities.[52] Therefore, the cocrystals of 5FU with these phenolic acids have potential synergistic antitumor effects. Comprehensive solid-state characterization techniques, such as X-ray diffraction, thermal analysis and dynamic vapor sorption measurements were carried out for all of the cocrystals. The aqueous solubility and dissolution behavior, as well as pharmacokinetic properties in rats were investigated.

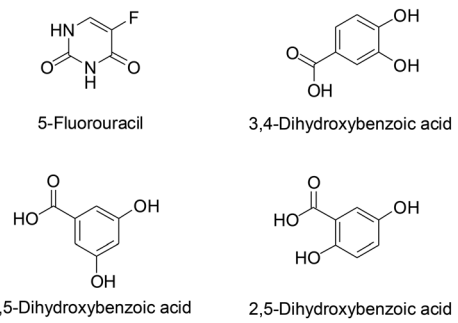

Scheme 1 Molecular structures of 5-fluorouracil and dihydroxybenzoic acids.

Experimental

Materials and general methods

5-Fluorouracil (5FU, purity >99%) was commercially available from Suizhou Hongqi Chemical Co. Ltd. 3,4-Dihydroxybenzoic acid (34DHBA), 3,5-dihydroxybenzoic acid (35DHBA) and 2,5-dihydroxybenzoic acid (25DHBA) were purchased from Aladdin Reagent Inc. All other chemicals and reagents were obtained from commercial suppliers and used directly. Powder X-ray diffraction (PXRD) measurements were performed at room temperature on a Bruker D2 Phaser with Cu Kα radiation (λ = 1.5418 Å) at 10 mA and 30 kV. Thermogravimetric (TG) analyses were conducted in a nitrogen atmosphere using a Netzsch TG 209F3 instrument. The sample was placed on an alumina crucible, and the temperature range of heating was from 30 to 500 °C at a heating rate of 10 °C min^{-1}. Differential scanning calorimetry (DSC) analyses were conducted on a Netzsch DSC 200 F3 instrument. The sample was placed on aluminum sample pans and heated in a nitrogen atmosphere from 30 °C to the decomposition temperature of the sample at a heating rate of 10 °C min^{-1}. Elemental analyses were carried out on an Elementar Vario EL Cube elemental analyzer.

Preparation of cocrystals

5FU–34DHBA, **5FU–35DHBA** and **5FU–25DHBA** were prepared by both liquid-assisted grinding and slurry methods. (1) A typical liquid-assisted grinding experiment was carried out by adding a stoichiometric amount of 5FU (130 mg, 1 mmol) and the corresponding CCFs with 20 μL of ethanol to a 25 mL stainless steel grinding jar. Then, the mixture was ground using a Retsch MM 200 mixer mill at a frequency of 20 Hz for 30 min. (2) Slurry experiments were performed by adding a mixture of 5FU (130 mg, 1 mmol) and the corresponding CCFs (154 mg, 1 mmol) to 1 mL of solvent. The resulting suspension was stirred for 24 h and filtered. The filter cake was dried at room temperature. **5FU–34DHBA·2H$_2$O** was prepared by a similar slurry method. The experimental parameters and yields of slurry, and elemental analyses of all the prepared cocrystal samples are summarized in Table 1. Bulk samples used for characterization and evaluation were obtained through the amplification of the slurry experiments.

Table 1 Slurry parameters, yields and elemental analyses of **5FU–34DHBA**, **5FU–34DHBA·2H$_2$O**, **5FU–35DHBA** and **5FU–25DHBA**

	5FU–34DHBA	5FU–34DHBA·2H$_2$O	5FU–35DHBA	5FU–25DHBA
Slurry solvent	Water	Water	Water	Water and ethanol (1 : 1)
Slurry temperature	50 °C	rt[a]	rt[a]	rt[a]
Yield (%)	80	76	88	87
Chemical formula	$C_{11}H_9FN_2O_6$	$C_{11}H_{13}FN_2O_8$	$C_{11}H_9FN_2O_6$	$C_{11}H_9FN_2O_6$
Anal. (%) calcd.	C, 46.49; H, 3.19; N, 9.86	C, 41.26; H, 4.09; N, 8.75	C, 46.49; H, 3.19; N, 9.86	C, 46.49; H, 3.19; N, 9.86
Anal. (%) found	C, 46.16; H, 3.55; N, 9.82	C, 40.80; H, 4.39; N, 8.81	C, 46.09; H, 3.46; N, 9.89	C, 46.05; H, 3.48; N, 10.29

[a] Room temperature.

Preparation of single crystals

Single crystals of **5FU–34DHBA·2H$_2$O**, **5FU–35DHBA** and **5FU–25DHBA** were obtained by adding 130 mg of 5FU and an equimolar amount of the corresponding CCFs into 2 mL of water and ethanol (1 : 1) and stirring for 1–2 h at 65 °C. The resulting hot suspensions were filtered, and the filtrates were cooled to room temperature. Pure 5FU crystals were precipitated at first, which were identified by PXRD and filtered to discard. The filtrates were then allowed to evaporate at room temperature for about one week to obtain single crystals of the cocrystals.

Single crystal X-ray diffraction (SCXRD)

SCXRD data of the cocrystals were collected at 150 K on an Agilent Technologies Gemini A Ultra system with graphite monochromated Cu Kα radiation (λ = 1.54178 Å). The program CrysAlis^{PRO} was applied for cell refinement and data reduction. The crystal structures were solved using the Olex-2 program by direct methods and refined through the full-matrix least-squares method on F^2. Hydrogen positions on the water molecule of **5FU–34DHBA·2H$_2$O** were located in Fourier-difference electron density maps. Other hydrogen atoms were placed in the calculated positions with fixed isotropic thermal parameters. All non-hydrogen atoms were refined by anisotropic displacement parameters.

Dynamic vapor sorption (DVS) study

DVS measurements were carried out using a DVS instrument (Surface Measurement Systems, UK). Well sieved powders (75–150 μm) of the cocrystals were placed on the sample pan and equilibrated at 0% relative humidity (RH) under a stream of nitrogen until the mass remained unchanged. Then, the RH of the sample room was programmatically controlled from 0% to 95% and back to 0% to run a cycle of adsorption and desorption processes in 10% RH steps. The temperature was maintained at 25 ± 0.1 °C during the measurement process. The sorption/desorption isotherms were obtained according to the equilibrium mass values.

Powder dissolution experiments

Powder dissolution experiments were carried out in water. 8 mL of water was added to a 25 mL flask and pre-heated at 37 °C for 30 min. Then, an excess of well sieved (75–150 μm) 5FU (320 mg) or the cocrystals (containing an equivalent amount of 5FU) was added. The resulting suspension was stirred at 150 rpm and 37 °C. An aliquot of the suspension was taken out using a syringe and filtered at each predetermined time interval. The filtrate was diluted 100 times and analyzed using HPLC to quantify the concentration of 5FU. After 8 h of dissolution experiments, the remaining solids were collected and detected by PXRD. The powder dissolution experiments were repeated three times for each sample (n = 3).

In vivo pharmacokinetic study

All the animal experiments were conducted according to institutional guidelines in compliance with the regulations formulated by Hebei Agricultural University. The experimental protocols were approved by the Institutional Animal Care and Use Committee of Hebei Agricultural University. Male Sprague-Dawley rats were purchased from SPF (Beijing) Biotechnology Co., Ltd. The rats weighing 220–270 g were fasted with free access to water for 12 h before drug administration. 5FU and all of the cocrystals were administered at a dose of 50 mg per kg body weight (the equivalent amount of free 5FU for the cocrystals). Well sieved samples with a particle size of 75–150 μm were dispersed in 1 mL of 0.5% sodium carboxymethylcellulose (CMC-Na) solution, and then administered by gavage. Blood samples were collected using heparinized injectors from the left or right retinal vein, at the following time intervals: 0, 0.083, 0.25, 0.5, 0.75, 1, 1.5, 2, 3, 4, 6, 8, 12 and 24 h after oral administration. The blood samples were centrifuged immediately at 6500 rpm for 10 min, and the separated plasmas were stored at −20 °C until analysis.

100 μL of plasma was added to 200 μL of 10% perchloric acid solution and the mixture was vortexed for 5 min and centrifuged at 10 000 rpm for 10 min. The supernatant was filtered with a 0.22 μm nylon membrane and analyzed by HPLC to quantify the concentration of 5FU. A standard curve was prepared to accurately quantify the concentration of 5FU in plasma. A 400 μg mL^{-1} stock solution of 5FU was prepared in water, and it was diluted to 200, 100, 50, 10, 5, 1 and 0.5 μg mL^{-1} with water. 10 μL of solution at each concentration was taken out and added into 90 μL of plasma. The mixture was vortexed for 5 min to obtain a group of 5FU plasma samples with gradient 5FU concentrations from 40 to 0.05 μg mL^{-1}.

Then, they were added into 200 μL of 10% perchloric acid solution and vortexed for 5 min, and subsequently centrifuged for 10 min. The supernatant was filtered and analyzed by HPLC. Each concentration was repeated for 5 groups. The result indicates that the standard curve was satisfied for the acceptance of the bioanalytical method ($R^2 > 0.999$).

Plasma drug concentration–time curves were fitted using DAS 2.0 software, and pharmacokinetic parameters such as C_{max}, t_{max}, MRT_{0-t}, $t_{1/2}$, and AUC_{0-t} were obtained. All the values were presented as mean ± S.D. for three rats.

HPLC analysis

HPLC analysis was conducted on a Shimadzu LC-2030C 3D Plus HPLC system with a UV detector. The detection wavelength of 5FU was set at 266 nm. In the powder dissolution study, a C18 column (Inertsil ODS-3, 5 μm × 4.6 mm × 150 mm column, GL Sciences Inc., Japan) at a column temperature of 30 °C was utilized for the HPLC analysis. The mobile phase was composed of methanol and a phosphoric acid aqueous solution (pH 2.4). Pure 5FU was analyzed by isocratic elution with 90% (v/v) phosphoric acid solution and 10% (v/v) methanol. **5FU–34DHBA**, **5FU–34DHBA·2H$_2$O**, **5FU–25DHBA** and **5FU–35DHBA** were analyzed by gradient elution, which was described as: 0–6 min, 10% (v/v) methanol; 6–8 min, from 10% to 60% (v/v) methanol; 8–15 min, 60% (v/v) methanol; 15–15.5 min, from 60% to 10% (v/v) methanol; 15.5–21 min, 10% (v/v) methanol. The flow rate was 0.7 mL min^{-1} for both isocratic and gradient elution.

In the *in vivo* pharmacokinetic study, another C18 column (XPeonyx C18-S, 5 μm × 4.6 mm × 250 mm column, FeiniGen Instruments Co., Ltd., China) at a column temperature of 30 °C was utilized for the HPLC analysis. Equivalent elution was used to separate 5FU and the CCFs. The mobile phase was a 0.01 mol L^{-1} potassium dihydrogen phosphate aqueous solution and the flow rate was set at 0.8 mL min^{-1}.

Table 2 Crystallographic data and refinement parameters for **5FU–34DHBA·2H$_2$O**, **5FU–35DHBA** and **5FU–25DHBA**

	5FU–34DHBA·2H$_2$O	5FU–35DHBA	5FU–25DHBA
Chemical formula	$C_{11}H_{13}FN_2O_8$	$C_{11}H_9FN_2O_6$	$C_{11}H_9FN_2O_6$
Formula wt	320.23	284.20	284.20
Temperature (K)	150.00(10)	150.00(10)	150.00(10)
Crystal size (mm^3)	0.1 × 0.05 × 0.03	0.1 × 0.05 × 0.02	0.1 × 0.08 × 0.02
Crystal system	Triclinic	Triclinic	Monoclinic
Space group	$P\bar{1}$	$P\bar{1}$	$P2_1/n$
a (Å)	7.2314(4)	7.8352(6)	9.5121(4)
b (Å)	9.9761(6)	8.9191(7)	5.5084(3)
c (Å)	10.2732(5)	9.4663(7)	21.2993(8)
α (deg)	103.754(5)	111.550(7)	90
β (deg)	102.275(5)	107.076(7)	94.115(4)
γ (deg)	108.186(5)	100.662(6)	90
Volume (Å^3)	650.05(7)	555.34(8)	1113.13(9)
Z	2	2	4
Density (g cm^{-3})	1.636	1.700	1.696
2θ range	4.662–63.677	5.471–79.650	4.162–67.265
F (000)	332	292	584
Index ranges	$-8 \le h \le 7$ $-11 \le k \le 11$ $-11 \le l \le 11$	$-9 \le h \le 7$ $-8 \le k \le 10$ $-11 \le l \le 12$	$-10 \le h \le 11$ $-6 \le k \le 5$ $-25 \le l \le 25$
No. of reflns	2111	2323	1995
No. of unique reflns	1783	2062	1712
No. of params	212	184	184
R_{all}, R_{obs}[a]	0.0484, 0.0404	0.0930, 0.0900	0.0469, 0.0393
w$R_{2,all}$, w$R_{2,obs}$[a]	0.1075, 0.0988	0.2295, 0.2227	0.1122, 0.1060
Goodness-of-fit on F^2	1.097	1.023	1.131
CCDC number	1970722	1970719	1970721

[a] $R_1 = \sum||F_o| - |F_c||/\sum|F_o|$. w$R_2 = [\sum[w(F_o^2 - F_c^2)^2]/\sum w(F_o^2)^2]^{1/2}$, $w = 1/[\sigma^2(F_o)^2 + (aP)^2 + bP]$, where $P = [(F_o^2) + 2F_c^2]/3$.

Results and discussion

Crystal structure analysis

SCXRD can provide a three-dimensional (3D) view of crystal structures and clarify the hydrogen bonding mode and molecular arrangement in crystals. The crystal structures of **5FU–34DHBA** and **5FU–25DHBA** determined at room temperature were published during the preparation of this article by Gautam *et al.*[38] In the current study, we solved the crystal structures of **5FU–34DHBA·2H$_2$O**, **5FU–35DHBA** and **5FU–25DHBA** at 150 K. The crystallographic data and refinement details are summarized in Table 2. Selected hydrogen bond distances and angles are presented in Table S1,† and the bond lengths and bond angles are given in Tables S2–S7.†

All of the cocrystals show different crystal structures due to the different positions of the carboxyl and hydroxyl groups of the aromatic ring in each CCF, which results in different hydrogen bonding modes between 5FU and the CCF in the cocrystals. As described in the literature,[38] the crystal structure of **5FU–34DHBA** belongs to the triclinic $P\bar{1}$ space group, with one molecule of 5FU and 34DHBA in the asymmetric unit. The 5FU molecules and 34DHBA molecules are connected to form a one-dimensional (1D) ribbon, with one amide group of the 5FU molecule connecting to the two phenolic hydroxyl groups of the 34DHBA molecule through double hydrogen bonds, and the oxygen atom on the other amide group of the 5FU molecule forming a hydrogen bond with the carboxyl group of the 34DHBA molecule. The adjacent 1D ribbons are further connected through hydrogen bonds between the carboxyl and hydroxyl groups of the 34DHBA molecules to form a two-dimensional (2D) sheet.

The crystal structure of **5FU–34DHBA·2H$_2$O** also belongs to the triclinic $P\bar{1}$ space group (Table 2). The asymmetric unit contains one 5FU molecule, one 34DHBA molecule and two water molecules (Fig. 1a). Two 5FU molecules are linked by double N2–H2B···O6 hydrogen bonds between the amide groups to generate a 5FU–5FU dimer (Fig. 1b). Two 34DHBA molecules are connected through double O4–H4···O1 hydrogen bonds between their phenolic hydroxyl and carboxyl groups to form a 34DHBA–34DHBA dimer (Fig. 1b).

The 5FU–5FU dimers and 34DHBA–34DHBA dimers are further connected to form a 1D ribbon *via* the N1–H1···O3 and N1–H1···O4 hydrogen bonds between 5FU and 34DHBA molecules as well as multiple hydrogen bonds (O7–H7A···O5, O2–H2···O7, O8–H8B···O6 and O8–H8A···O7) with the water molecules involved (Fig. 1b). Neighboring ribbons are further united through the O3–H3···O8 hydrogen bonds between water and 34DHBA molecules to generate a 2D sheet (Fig. 1b). Adjacent 2D sheets are then packed *via* the O7–H7B···O8 hydrogen bonds between water molecules and the intersheet π···π interactions (3.864 Å) to form a 3D structure (Fig. 1c and d).

5FU–35DHBA crystallizes in the triclinic $P\bar{1}$ space group, with one 5FU molecule and one 35DHBA molecule in the asymmetric unit (Table 2 and Fig. 2a). Two 5FU molecules are connected through an amide–amide homosynthon (N1–H1···O1) to generate a 5FU–5FU dimer, and two 35DHBA molecules are linked by double O3–H3···O5 hydrogen bonds to form a 35DHBA–35DHBA dimer (Fig. 2b). The 5FU–5FU dimers and 35DHBA–35DHBA dimers are then connected *via*

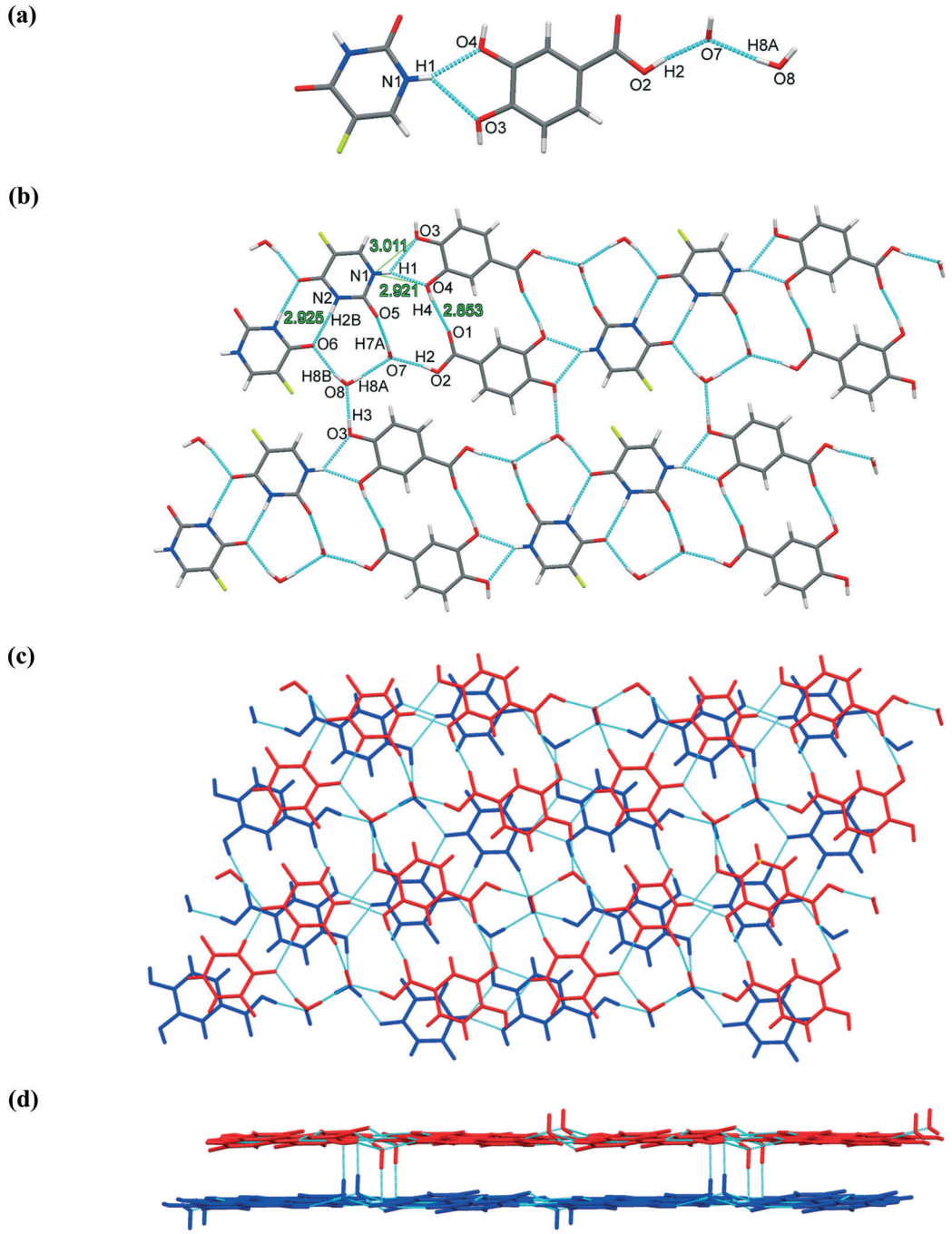

Fig. 1 (a) 5FU–34DHBA·2H_2O unit, (b) 2D sheet structure, and (c) vertical view and (d) side view of the 3D structure in **5FU–34DHBA·2H_2O**.

an amide–acid heterosynthon (N2–H2···O5 and O6–H6···O1) to form a 1D ribbon (Fig. 2b). Neighboring ribbons are further united through the O4–H4···O2 hydrogen bonds between 5FU and 35DHBA molecules to generate a 2D layer (Fig. 2b). Adjacent 2D layers are further packed through van der Waals interactions to form a 3D structure (Fig. 2c and d).

The crystal structure of **5FU–25DHBA** was solved at 150 K in the present study, which shows similar cell parameters and slightly reduced dimensions compared with the crystallographic data obtained at room temperature.[38] The crystal structure of **5FU–25DHBA** is distinguished from those of the three cocrystals described above, which belongs to the monoclinic $P2_1/n$ space group and shows a different molecular arrangement and packing pattern. The asymmetric unit contains one 5FU molecule and one 25DHBA molecule (Table 2 and Fig. 3a). One molecule of 5FU and 25DHBA are connected through the O4–H4A···O6 hydrogen bond to form a 5FU–25DHBA dimer (Fig. 3b). Two 5FU–25DHBA dimers are connected head-to-tail through the N1–H1···O4 hydrogen bonds to form a tetramer, and the tetramers are further united *via* the N2–H2A···O1 and O2–H2···O5 hydrogen bonds between 5FU molecules and 25DHBA molecules to form a 1D

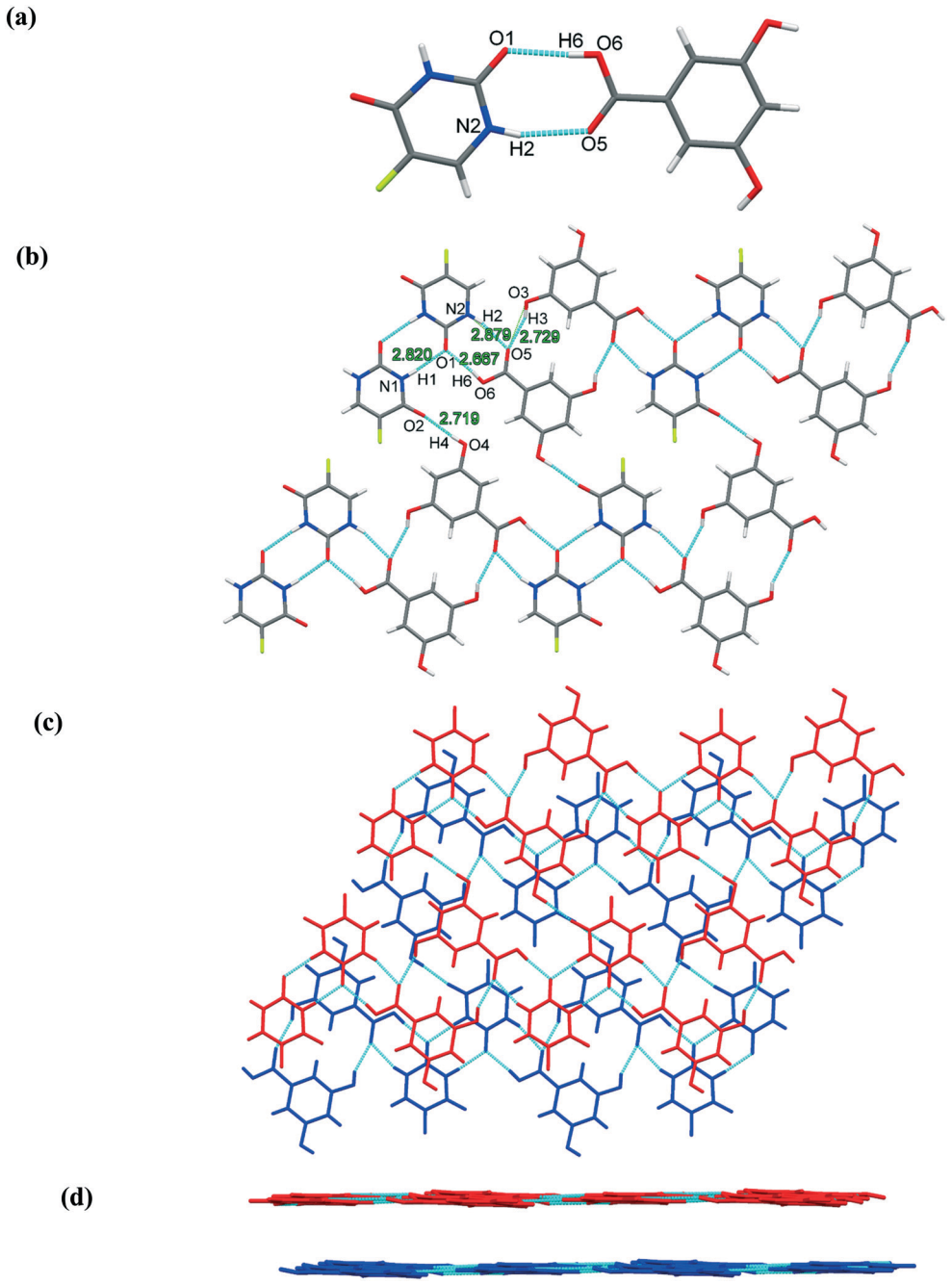

Fig. 2 (a) 5FU–35DHBA unit, (b) 2D sheet structure, and (c) vertical view and (d) side view of the 3D structure in **5FU–35DHBA**.

ribbon (Fig. 3b). The ribbons are not united to form a 2D layer like those in the three cocrystals mentioned above, but are staggered in different directions to pack into the entire 3D structure of **5FU–25DHBA** *via* van der Waals interactions (Fig. 3c and d).

PXRD analysis

PXRD was used to determine the crystal form and phase purity of the bulk samples of the cocrystals. From Fig. 4, it can be seen that all the PXRD patterns of the cocrystals are different from those of their parent materials, and the characteristic peaks of the parent materials disappear after cocrystallization, suggesting the successful synthesis of cocrystals. For **5FU–34DHBA**, the measured PXRD pattern is consistent with the published pattern, confirming the purity of the bulk sample.[38] For **5FU–34DHBA·2H$_2$O**, **5FU–35DHBA** and **5FU–25DHBA**, the experimental PXRD patterns closely match the simulated patterns from the SCXRD data, indicating that the bulk crystalline samples correspond to the respective single crystal structures (Fig. 4). The slight discrepancy between the simulated and experimental patterns in the high angle regions is mainly due to the different test temperatures of SCXRD (150 K) and PXRD (room temperature).

Thermal analysis

The thermodynamic stability of all the cocrystals was investigated by TG and DSC analyses (Fig. S1†). **5FU–34DHBA**, **5FU–35DHBA** and **5FU–25DHBA** began to decompose at approximately 220 °C, 243 °C and 211 °C, respectively, and

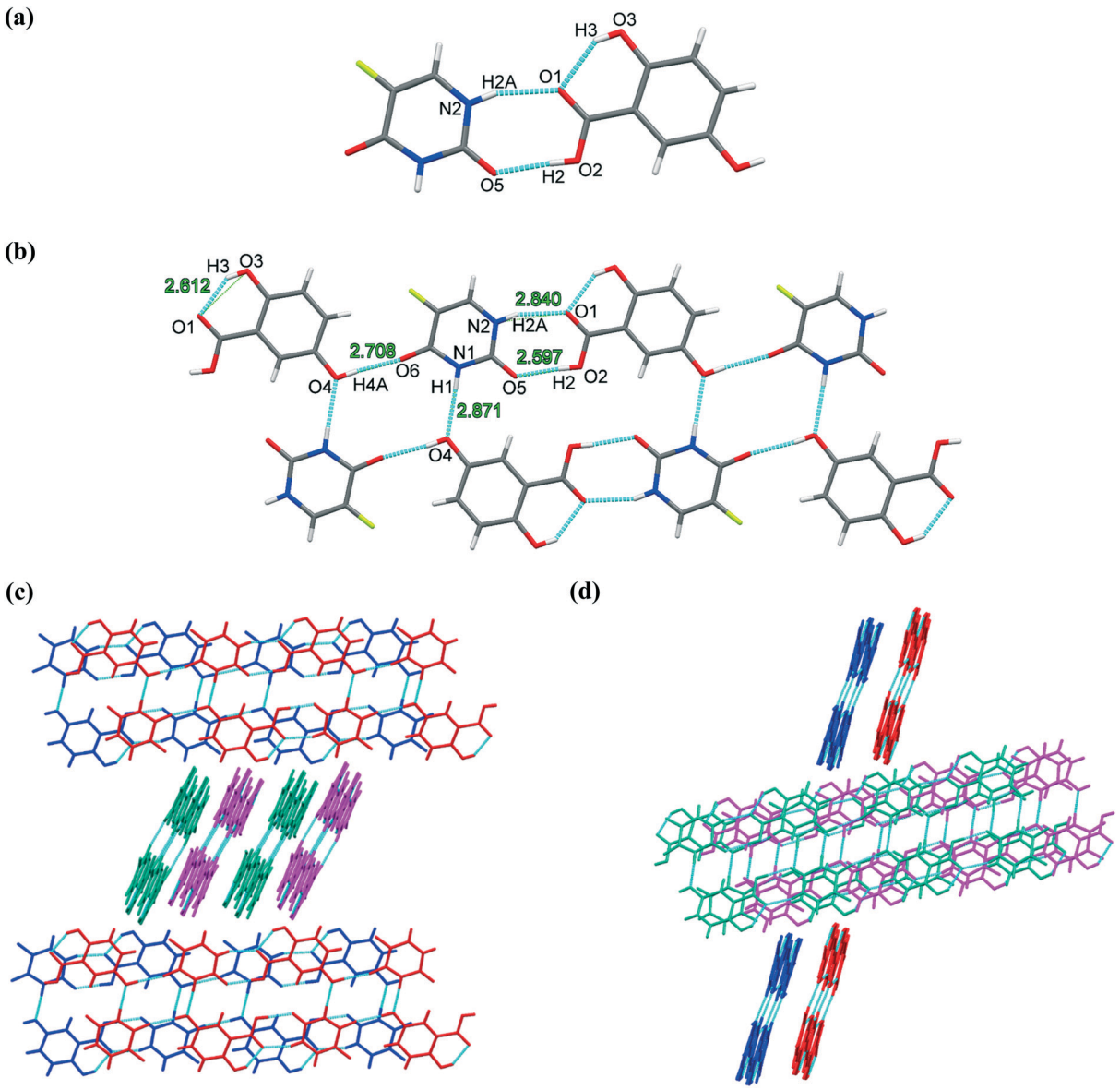

Fig. 3 (a) 5FU–25DHBA unit, (b) 2D sheet structure, and (c) vertical view and (d) side view of the 3D structure in **5FU–25DHBA**.

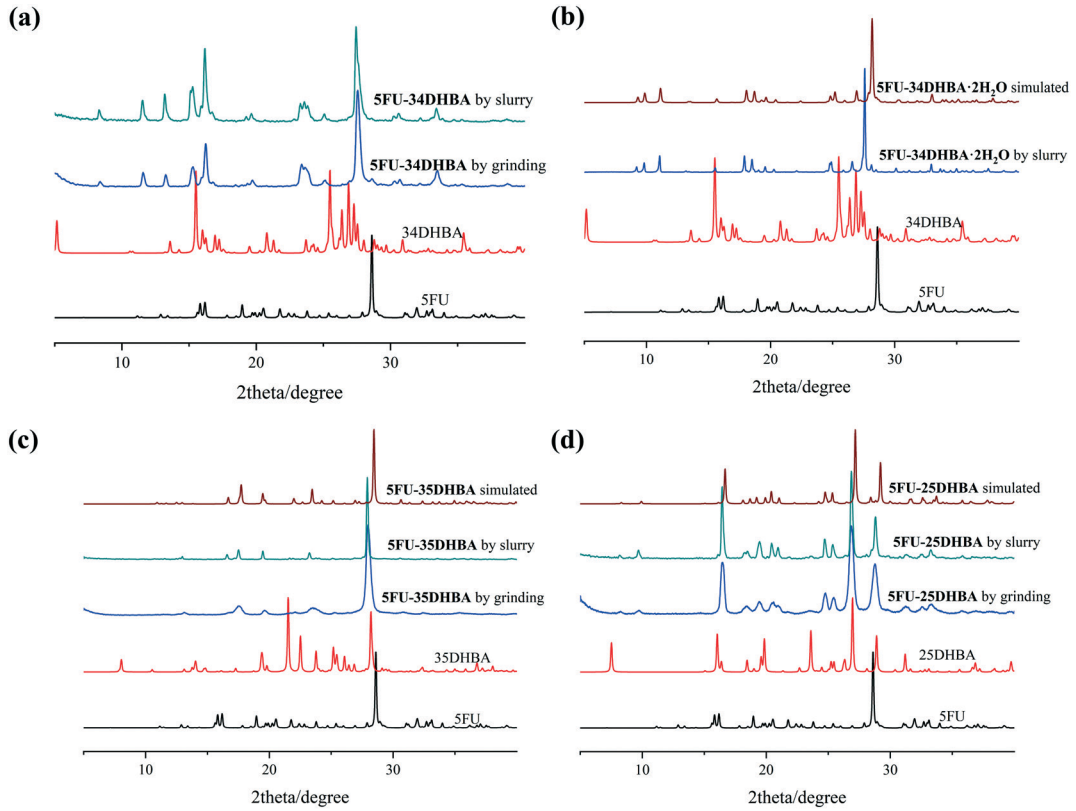

Fig. 4 PXRD patterns of 5FU, the corresponding CCFs, and the as-synthesized samples (and those simulated from the single crystal data) for (a) **5FU–34DHBA**, (b) **5FU–34DHBA·2H$_2$O**, (c) **5FU–35DHBA** and (d) **5FU–25DHBA**.

there is no endothermic or exothermic signal observed in the DSC curves before the decomposition temperature, indicating that the samples decompose directly without phase transformation. The TG curve of **5FU–34DHBA·2H$_2$O** evidenced a weight loss of 11.4% from 38 to 67 °C, which corresponds to the weight loss of two water molecules (calcd. 11.2%). The DSC curve of **5FU–34DHBA·2H$_2$O** demonstrated an endothermic peak derived from the dehydration process and no other enthalpy change before the decomposition temperature. In order to verify the crystalline phase of the powder after losing water, the sample of **5FU–34DHBA·2H$_2$O** was heated to 80 °C, and then cooled to room temperature and measured by PXRD. The result indicates that **5FU–34DHBA·2H$_2$O** was dehydrated upon heating forming the anhydrous form, **5FU–34DHBA** (Fig. S2†).

DVS study

DVS experiments were performed to investigate the hygroscopicity of the cocrystals. The obtained vapor sorption/desorption isotherms are displayed in Fig. 5. The results show that **5FU–34DHBA**, **5FU–35DHBA** and **5FU–25DHBA** absorbed 0.07%, 0.10% and 0.03% of water at 95% RH, respectively, which can be regarded as surface adsorption.[20] In the desorption process, the three cocrystals lost their adsorbed water and returned to the initial state to form a closed sorption/desorption curve, indicating that no phase transformation occurred during the DVS experiments, which were further proved by PXRD tests (Fig. S3†). In contrast, **5FU–34DHBA·2H$_2$O** lost two water molecules (about 11.0% in mass) in the initial equilibrium stage under 0% RH, and the dehydrated sample was proved to be anhydrous **5FU–34DHBA** by PXRD (Fig. S3†). During the adsorption process, the dehydrated sample absorbed 0.15% of water until 95% RH and returned to the initial state of anhydrous **5FU–34DHBA** in the desorption process to form a closed sorption–desorption curve. The slightly increased adsorption at 95% RH compared to that for **5FU–34DHBA** (0.07%) may be due to the decreased crystallinity after dehydration. It is noteworthy that the dehydrated sample of **5FU–34DHBA·2H$_2$O** did not restore to the dihydrate form during the adsorption process (Fig. S3†), suggesting that **5FU–34DHBA** is the relatively more stable form toward humidity variation as compared to **5FU–34DHBA·2H$_2$O**.

Phase transformation study

In the present study, a pair of anhydrous and dihydrate cocrystals, **5FU–34DHBA** and **5FU–34DHBA·2H$_2$O**, is involved. The crystalline phase transformation between **5FU–34DHBA** and **5FU–34DHBA·2H$_2$O** was investigated under different conditions. Fig. 6 summarizes their mutual transformation diagram. **5FU–34DHBA·2H$_2$O** was prepared by adding equimolar amounts of 5FU and 34DHBA in water and stirring

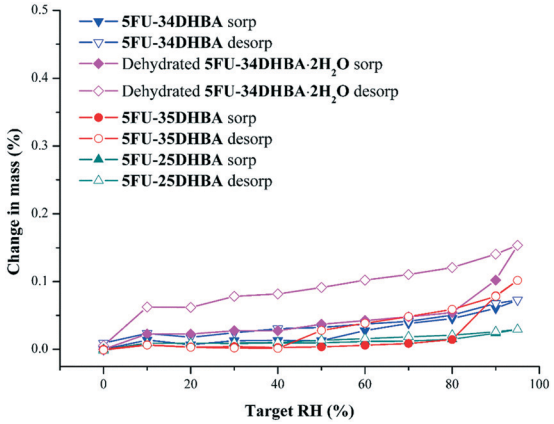

Fig. 5 DVS isotherm plots of the 5FU cocrystals.

at room temperature, while **5FU–34DHBA** was synthesized at 50 °C through a similar slurry method. **5FU–34DHBA·2H$_2$O** is sensitive to heat and humidity. It will lose two crystal water molecules to form **5FU–34DHBA** when heated to 80 °C or equilibrated at 0% humidity. In comparison, **5FU–34DHBA** is stable against heat and humidity. However, **5FU–34DHBA** is dynamically unstable and changes into **5FU–34DHBA·2H$_2$O** when stirred in water at room temperature.

Aqueous solubility

The powder dissolution profiles of 5FU and its cocrystals in water are graphed in Fig. 7. The maximum apparent solubility (S_{max}) of 5FU and its cocrystals is summarized in Table 3. The results show that 5FU, **5FU–34DHBA·2H$_2$O**, **5FU–35DHBA** and **5FU–25DHBA** reached the S_{max} quickly and maintained a stable concentration of 5FU during the remaining dissolution process. In contrast, after **5FU–34DHBA** reached the S_{max} at about 10 min, the drug concentration kept decreasing until it was equal to that of **5FU–34DHBA·2H$_2$O**. This suggests that **5FU–34DHBA** was unstable and may have gradually transformed into **5FU–34DHBA·2H$_2$O** during the dissolution process. The S_{max} of pure 5FU, **5FU–34DHBA**, **5FU–34DHBA·2H$_2$O**, **5FU–35DHBA** and **5FU–25DHBA** was 17.29 ± 0.40, 23.23 ± 0.31, 19.27 ± 0.27, 12.57 ± 0.16 and 8.53 ± 0.26 mg mL^{-1}, respectively, with the order **5FU–34DHBA** > **5FU–34DHBA·2H$_2$O** > 5FU > **5FU–35DHBA** > **5FU–25DHBA**. As compared to pure 5FU, the S_{max} values of **5FU–34DHBA** and **5FU–34DHBA·2H$_2$O** were increased by 34% and 11% while those of **5FU–35DHBA** and **5FU–25DHBA** were reduced by 27% and 51%, respectively. The PXRD patterns of the resulting solids after the dissolution experiments show that the crystalline form of all the cocrystals remained unchanged except that for **5FU–34DHBA**, which transformed into **5FU–34DHBA·2H$_2$O** (Fig. S4†). This is consistent with the dissolution curves (Fig. 7).

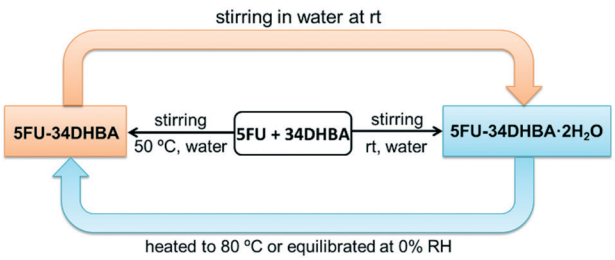

Fig. 6 Phase transformation diagram of **5FU–34DHBA** and **5FU–34DHBA·2H$_2$O** (rt corresponds to room temperature).

Solubility–structure relationship

The different solubility of cocrystals may be related to their different crystal packing. **5FU–34DHBA**, **5FU–34DHBA·2H$_2$O** and **5FU–35DHBA** exhibit great similarities in hydrogen bonded layer structures and the packing modes of these layers whereas **5FU–25DHBA** shows totally different crystal packing, in which the one-dimensional ribbons are staggered in two directions with a dihedral angle of 70° to pack into a three-dimensional structure. **5FU–25DHBA** demonstrates the lowest solubility due to this distinct and efficient crystal packing mode. As compared to **5FU–34DHBA**, **5FU–34DHBA·2H$_2$O** contains more hydrogen bonding interactions due to the presence of water molecules in the crystal lattice, thus showing relatively lower solubility. When comparing **5FU–34DHBA·2H$_2$O** and **5FU–35DHBA**, the latter exhibits more efficient crystal packing with a closer interlayer distance of 3.145 Å (*vs.* 3.171 Å for **5FU–34DHBA·2H$_2$O**), which is consistent with the fact that **5FU–35DHBA** is less soluble than **5FU–34DHBA·2H$_2$O**.

Pharmacokinetics study

The cocrystallization approach is often used to improve the solubility of insoluble drugs to improve their oral bioavailability. Only limited studies have focused on employing cocrystallization to reduce the solubility of highly soluble drugs to extend the *in vivo* retention time and subsequently improve their oral absorption.[30,31] 5FU is an effective and commonly used antineoplastic drug with good

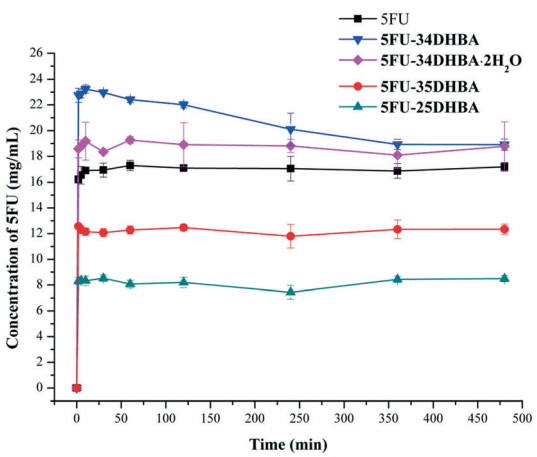

Fig. 7 Dissolution profiles of 5FU and its cocrystals against time in water at 37 °C.

Table 3 Maximum apparent solubility and pharmacokinetic parameters following oral administration of free 5FU and its cocrystals to male rats

Parameters	5FU	5FU–34DHBA	5FU–34DHBA·2H$_2$O	5FU–35DHBA	5FU–25DHBA
S_{max} (mg mL^{-1})	17.29 ± 0.40	23.23 ± 0.31	19.27 ± 0.27	12.57 ± 0.16	8.53 ± 0.26
C_{max} (μg mL^{-1})	14.34 ± 3.01	29.62 ± 20.77	16.72 ± 8.58	6.16 ± 1.47	1.90 ± 0.60
t_{max} (h)	0.75 ± 0.00	0.14 ± 0.10	0.19 ± 0.10	1.08 ± 0.88	1.00 ± 0.90
MRT$_{0-t}$ (h)	0.93 ± 0.05	4.94 ± 2.25	8.11 ± 2.67	5.35 ± 1.62	9.08 ± 0.22
$t_{1/2}$ (h)	0.34 ± 0.12	3.89 ± 0.44	8.86 ± 5.24	6.75 ± 4.12	11.40 ± 5.55
AUC$_{0-t}$ (μg h mL^{-1})	9.30 ± 3.19	22.13 ± 9.49	16.29 ± 1.77	13.81 ± 0.72	10.43 ± 1.04

solubility. The half-life of 5FU is very short with a severe peak-valley effect.[53] To maintain adequate blood drug concentration, oral 5FU always requires frequent administration at large doses, which further results in serious side effects and undesirable drug resistance.[1]

In order to investigate whether the solubility alteration of 5FU caused by cocrystallization can be converted into an *in vivo* pharmacokinetic advantage, 5FU and its cocrystals were orally administered to male rats at a dose of 50 mg kg^{-1} 5FU. The plasma drug concentration–time profiles are graphed in Fig. 8 with each cocrystal separately displayed against the 5FU control. The corresponding pharmacokinetic parameters are summarized in Table 3.

For the parent 5FU, the plasma concentration reached its peak at 0.75 h with a C_{max} value of 14.34 ± 3.01 μg mL^{-1}. The 5FU plasma concentrations were undetectable after 2 h with a MRT$_{0-t}$ value of 0.93 ± 0.05 h, and its $t_{1/2}$ value was only 0.34 ± 0.12 h. The rapid elimination of 5FU herein is consistent with the results reported in the literature, which showed a $t_{1/2}$ value of 0.36 ± 0.09 h and undetectable 5FU concentration after 4 h.[13] In general, the rapid elimination of 5FU leads to its low bioavailability, with an AUC$_{0-t}$ value of 9.30 ± 3.19 μg h mL^{-1}.

Compared to the parent 5FU, all the cocrystals exhibited totally different pharmacokinetic parameters (Table 3). The C_{max} of **5FU–34DHBA**, **5FU–34DHBA·2H$_2$O**, **5FU–35DHBA** and **5FU–25DHBA** was respectively modified to 29.62 ± 20.77, 16.72 ± 8.58, 6.16 ± 1.47 and 1.90 ± 0.60 μg mL^{-1}, with the order **5FU–34DHBA** > **5FU–34DHBA·2H$_2$O** > 5FU > **5FU–35DHBA** > **5FU–25DHBA**, which is in agreement with their aqueous solubilities. The t_{max} values of the cocrystals were modulated to 0.14–1.08 h and ordered as follows: **5FU–**

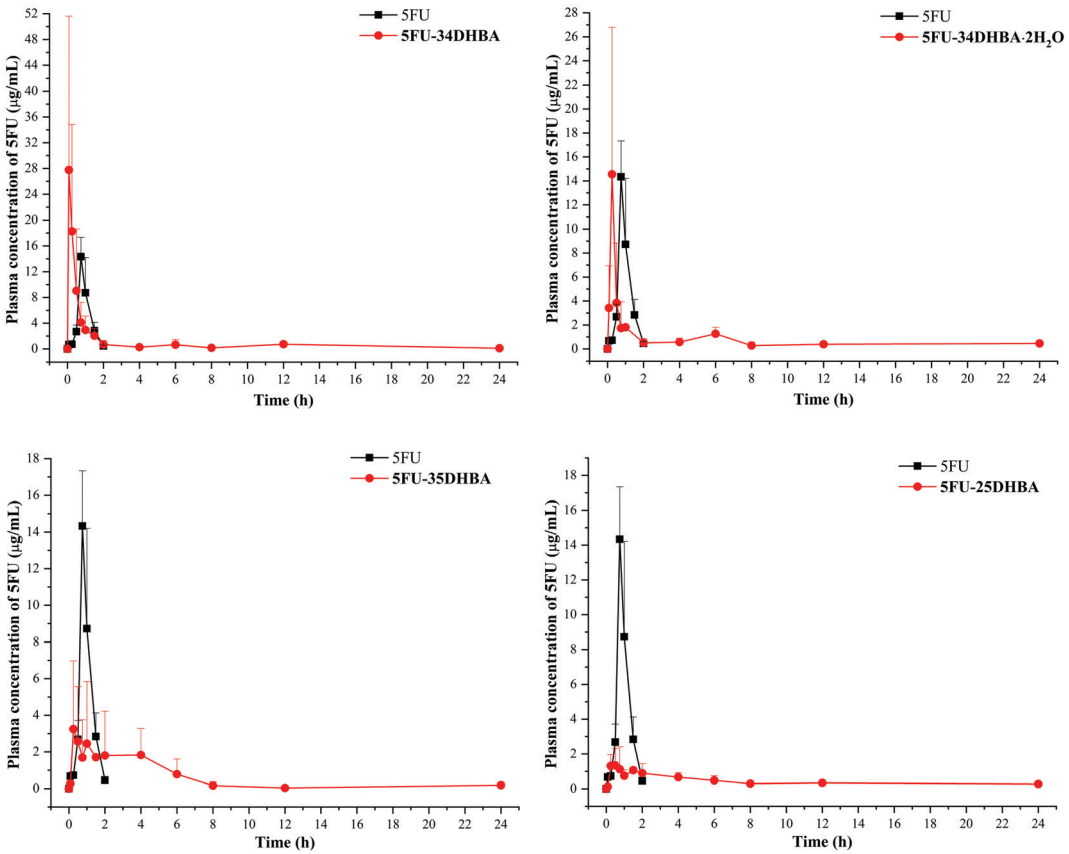

Fig. 8 Mean plasma 5FU concentrations *versus* time profiles following oral administration of free 5FU and its cocrystals to male rats. Each point represents the mean ± SD (n = 3).

34DHBA < **5FU–34DHBA·2H$_2$O** < 5FU < **5FU–25DHBA** < **5FU–35DHBA**, which is negatively correlated with the order of their dissolution rates. This suggested that the alteration of solubility and dissolution rates by cocrystal formation could further convert to the modification of the C_{max} and t_{max} values of the drug. In the current research, the cocrystals with better solubility and dissolution rates exhibit greater C_{max} and a faster time to peak and *vice versa*. Besides, the MRT_{0-t} and $t_{1/2}$ values were respectively extended to 4.94–9.08 and 3.89–11.40 h for the different cocrystals, and the AUC_{0-t} was 22.13 ± 9.49, 16.29 ± 1.77, 13.81 ± 0.72 and 10.43 ± 1.04 μg h mL^{-1} for **5FU–34DHBA**, **5FU–34DHBA·2H$_2$O**, **5FU–35DHBA** and **5FU–25DHBA**, respectively (Table 3).

In addition, cocrystal formation also modified the shape of the plasma drug concentration–time profiles. 5FU peaked rapidly and was eliminated within 2 h with severe peak-valley effects when orally administered. **5FU–34DHBA** and **5FU–34DHBA·2H$_2$O** have higher C_{max} values and a faster time to peak; thus, the AUC_{0-t} values of **5FU–34DHBA** and **5FU–34DHBA·2H$_2$O** were effectively enhanced, with a 2.38 and 1.75 times improvement in comparison with that of free 5FU (Table 3). However, their plasma drug concentrations demonstrated a severer peak-valley effect, which may aggravate the side effects of the drug. In contrast, **5FU–35DHBA** and **5FU–25DHBA** exhibited lower C_{max} values and a delayed time to peak. It is noteworthy that unlike that of pure 5FU, the pharmacokinetic curves of **5FU–35DHBA** and **5FU–25DHBA** had no obvious peak-valley phenomena, but exhibited a sustained plateau with different levels of plasma drug concentration. After that, the plasma concentrations of 5FU decreased slowly until 24 h. Although the AUC_{0-t} values of **5FU–35DHBA** and **5FU–25DHBA** are comparable to that of free 5FU, the sustained 5FU concentrations in the blood could be useful for avoiding the peak-valley effect and frequent administration. This is of great significance to reduce the side effects and drug resistance of 5FU and make it potential to be orally administrated in the clinical practice.

Conclusions

In the present study, the cocrystallization of 5FU was utilized to modulate the pharmacokinetic properties of 5FU by altering its aqueous solubility and dissolution rate. Four cocrystals of 5FU with a group of DHBAs were synthesized and characterized, namely **5FU–34DHBA** (1 : 1), **5FU–35DHBA** (1 : 1), **5FU–25DHBA** (1 : 1) and **5FU–34DHBA·2H$_2$O** (1 : 1 : 2). All the cocrystals exhibit different aqueous solubilities and *in vivo* pharmacokinetic behaviors as compared to pure 5FU. **5FU–34DHBA** and **5FU–34DHBA·2H$_2$O** demonstrate a faster time to peak, and higher C_{max} and AUC_{0-t} due to their increased dissolution rates and solubility. In contrast, **5FU–25DHBA** and **5FU–35DHBA** exhibit a delayed peak time, lower C_{max} and comparable AUC_{0-t} with a sustained plasma drug concentration plateau attributed to the reduced dissolution rates and solubility, which is helpful to overcome the peak-valley effect and frequent administration requirement of 5FU, and further reduce the side effects and drug resistance. This study has important implications for using the cocrystallization approach to ameliorate the pharmacokinetic properties of drugs with undesirable oral absorption in clinical practice.

Conflicts of interest

There are no conflicts to declare.

Acknowledgements

This work was financially supported by the National Natural Science Foundation of China (grant numbers 21571194 and 31872508).

Notes and references

1 R. B. Diasio and B. E. Harris, Clinical pharmacology of 5-fluorouracil, *Clin. Pharmacokinet.*, 1989, **16**, 215–237.
2 D. B. Longley, D. P. Harkin and P. G. Johnston, 5-Fluorouracil: mechanisms of action and clinical strategies, *Nat. Rev. Cancer*, 2003, **3**, 330–338.
3 W. Kelder, G. A. P. Hospers and J. T. M. Plukker, Effects of 5-fluorouracil adjuvant treatment of colon cancer, *Expert Rev. Anticancer Ther.*, 2006, **6**, 785–794.
4 J. S. Y. Ng, D. A. Cameron and R. C. F. Leonard, Infusional 5-fluorouracil in breast cancer, *Cancer Treat. Rev.*, 1994, **20**, 357–364.
5 S. Sato, H. Itamochi, J. Kigawa, T. Oishi, M. Shimada, S. Sato, J. Naniwa, K. Uegaki, M. Nonaka and N. Terakawa, Combination chemotherapy of oxaliplatin and 5-fluorouracil may be an effective regimen for mucinous adenocarcinoma of the ovary: a potential treatment strategy, *Cancer Sci.*, 2009, **100**, 546–551.
6 D. A. Askew, S. M. Mickan, H. P. Soyer and D. Wilkinson, Effectiveness of 5-fluorouracil treatment for actinic keratosis–a systematic review of randomized controlled trials, *Int. J. Dermatol.*, 2009, **48**, 453–463.
7 R. I. Ceilley, Mechanisms of action of topical 5-fluorouracil: review and implications for the treatment of dermatological disorders, *J. Dermatol. Treat.*, 2012, **23**, 83–89.
8 N. Sanoj Rejinold, K. P. Chennazhi, S. V. Nair, H. Tamura and R. Jayakumar, Biodegradable and thermo-sensitive chitosan-g-poly (N-vinylcaprolactam) nanoparticles as a 5-fluorouracil carrier, *Carbohydr. Polym.*, 2011, **83**, 776–786.
9 F. Farshi Azhar and A. Olad, A study on sustained release formulations for oral delivery of 5-fluorouracil based on alginate-chitosan/montmorillonite nanocomposite systems, *Appl. Clay Sci.*, 2014, **101**, 288–296.
10 Y. Huang, Y. Wei, H. Yang, C. Pi, H. Liu, Y. Ye and L. Zhao, A 5-fluorouracil-loaded floating gastroretentive hollow microsphere: development, pharmacokinetic in rabbits, and biodistribution in tumor-bearing mice, *Drug Des., Dev. Ther.*, 2016, **10**, 997–1008.
11 A. Bose, A. Elyagoby and T. W. Wong, Oral 5-fluorouracil colon-specific delivery through in vivo pellet coating for

colon cancer and aberrant crypt foci treatment, *Int. J. Pharm.*, 2014, **468**, 178–186.

12 A. Chen, Y. Shi, Z. Q. Yan, H. X. Hao, Y. Zhang, J. Zhong and H. M. Hou, Dosage form developments of nanosuspension drug delivery system for oral administration route, *Curr. Pharm. Des.*, 2015, **21**, 4355–4365.

13 X. Li, Y. Xu, G. Chen, P. Wei and Q. Ping, PLGA nanoparticles for the oral delivery of 5-fluorouracil using high pressure homogenization-emulsification as the preparation method and in vitro/in vivo studies, *Drug Dev. Ind. Pharm.*, 2008, **34**, 107–115.

14 A. C. de Mattos, C. Altmeyer, T. T. Tominaga, N. M. Khalil and R. M. Mainardes, Polymeric nanoparticles for oral delivery of 5-fluorouracil: formulation optimization, cytotoxicity assay and pre-clinical pharmacokinetics study, *Eur. J. Pharm. Sci.*, 2016, **84**, 83–91.

15 P. Pal, J. P. Pandey and G. Sen, Sesbania gum based hydrogel as platform for sustained drug delivery: an "in vitro" study of 5-Fu release, *Int. J. Biol. Macromol.*, 2018, **113**, 1116–1124.

16 X. L. Dai, J. M. Chen and T. B. Lu, Pharmaceutical cocrystallization: an effective approach to modulate the physicochemical properties of solid-state drugs, *CrystEngComm*, 2018, **20**, 5292–5316.

17 J. R. Wang, X. J. Wang, Y. Yang, X. Y. Chen and X. F. Mei, Solid-state characterization of 17β-estradiol co-crystals presenting improved dissolution and bioavailability, *CrystEngComm*, 2016, **18**, 3498–3505.

18 A. Dalpiaz, V. Ferretti, V. Bertolasi, B. Pavan, A. Monari and M. Pastore, From physical mixtures to co-crystals: how the coformers can modify solubility and biological activity of carbamazepine, *Mol. Pharmaceutics*, 2018, **15**, 268–278.

19 T. C. Machado, A. B. Gelain, J. Rosa, S. G. Cardoso and T. Caon, Cocrystallization as a novel approach to enhance the transdermal administration of meloxicam, *Eur. J. Pharm. Sci.*, 2018, **123**, 184–190.

20 R. Z. Lin, P. J. Sun, Q. Tao, J. Yao, J. M. Chen and T. B. Lu, Mechanism study on stability enhancement of adefovir dipivoxil by cocrystallization: degradation kinetics and structure-stability correlation, *Eur. J. Pharm. Sci.*, 2016, **85**, 141–148.

21 J. H. Deng, T. B. Lu, C. C. Sun and J. M. Chen, Dapagliflozin-citric acid cocrystal showing better solid state properties than dapagliflozin, *Eur. J. Pharm. Sci.*, 2017, **104**, 255–261.

22 C. Wang, S. Paul, K. Wang, S. Hu and C. C. Sun, Relationships among crystal structures, mechanical properties, and tableting performance probed using four salts of diphenhydramine, *Cryst. Growth Des.*, 2017, **17**, 6030–6040.

23 R. Khatioda, B. Saikia, P. J. Das and B. Sarma, Solubility and in vitro drug permeation behaviour of ethenzamide cocrystals regulated in physiological pH environments, *CrystEngComm*, 2017, **19**, 6992–7000.

24 K. Suresh and A. Nangia, Curcumin: pharmaceutical solids as a platform to improve solubility and bioavailability, *CrystEngComm*, 2018, **20**, 3277–3296.

25 Y. Chen, L. Li, J. Yao, Y. Y. Ma, J. M. Chen and T. B. Lu, Improving the solubility and bioavailability of apixaban via apixaban-oxalic acid cocrystal, *Cryst. Growth Des.*, 2016, **16**, 2923–2930.

26 C. Liu, Z. Liu, Y. Chen, Z. Chen, H. Chen, Y. Pui and F. Qian, Oral bioavailability enhancement of β-lapachone, a poorly soluble fast crystallizer, by cocrystal, amorphous solid dispersion, and crystalline solid dispersion, *Eur. J. Pharm. Biopharm.*, 2018, **124**, 73–81.

27 R. Sa, Y. Zhang, Y. Deng, Y. Huang, M. Zhang and B. Lou, Novel salt cocrystal of chrysin with berberine: preparation, characterization, and oral bioavailability, *Cryst. Growth Des.*, 2018, **18**, 4724–4730.

28 N. Shan, M. L. Perry, D. R. Weyna and M. J. Zaworotko, Impact of pharmaceutical cocrystals: the effects on drug pharmacokinetics, *Expert Opin. Drug Metab. Toxicol.*, 2014, **10**, 1255–1271.

29 M. Rodrigues, B. Baptista, J. A. Lopes and M. C. Sarraguça, Pharmaceutical cocrystallization techniques. Advances and challenges, *Int. J. Pharm.*, 2018, **547**, 404–420.

30 S. Aitipamula, J. Cadden and P. S. Chow, Cocrystals of zonisamide: physicochemical characterization and sustained release solid forms, *CrystEngComm*, 2018, **20**, 2923–2931.

31 J. M. Chen, S. Li and T. B. Lu, Pharmaceutical cocrystals of ribavirin with reduced release rates, *Cryst. Growth Des.*, 2014, **14**, 6399–6408.

32 A. J. Smith, P. Kavuru, K. K. Arora, S. Kesani, J. Tan, M. J. Zaworotko and R. D. Shytle, Crystal engineering of green tea epigallocatechin-3-gallate (EGCg) cocrystals and pharmacokinetic modulation in rats, *Mol. Pharmaceutics*, 2013, **10**, 2948–2961.

33 C. Almansa, R. Mercè, N. Tesson, J. Farran, J. Tomàs and C. R. Plata-Salamán, Co-crystal of tramadol hydrochloride-celecoxib (CTC): a novel API-API co-crystal for the treatment of pain, *Cryst. Growth Des.*, 2017, **17**, 1884–1892.

34 A. V. Yadav, A. S. Shete, A. P. Dabke, P. V. Kulkarni and S. S. Sakhare, Co-crystals: a novel approach to modify physicochemical properties of active pharmaceutical ingredients, *Indian J. Pharm. Sci.*, 2009, **71**, 359–370.

35 B. B. Eedara, I. G. Tucker, Z. D. Zujovic, T. Rades, J. R. Price and S. C. Das, Crystalline adduct of moxifloxacin with trans-cinnamic acid to reduce the aqueous solubility and dissolution rate for improved residence time in the lungs, *Eur. J. Pharm. Sci.*, 2019, **136**, 104961.

36 X. L. Dai, A. P. Voronin, W. Gao, G. L. Perlovich, T. B. Lu and J. M. Chen, Intermolecular interactions and permeability of 5-fluorouracil cocrystals with a series of isomeric hydroxybenzoic acids: a combined theoretical and experimental study, *CrystEngComm*, 2019, **21**, 5095–5105.

37 A. C. Williams and B. W. Barry, Terpenes and the lipidprotein partitioning theory of the skin penetration enhancement, *Pharm. Res.*, 1991, **8**, 17–24.

38 M. K. Gautam, M. Besan, D. Pandit, S. Mandal and R. Chadha, Cocrystal of 5-fluorouracil: characterization and evaluation of biopharmaceutical parameters, *AAPS PharmSciTech*, 2019, **20**, 149.

39 X. L. Dai, S. Li, J. M. Chen and T. B. Lu, Improving the membrane permeability of 5-fluorouracil via cocrystallization, *Cryst. Growth Des.*, 2016, **16**, 4430–4438.

40 X. L. Dai, A. P. Voronin, Y. L. Huang, G. L. Perlovich, X. H. Zhao, T. B. Lu and J. M. Chen, 5-Fluorouracil cocrystals with lipophilic hydroxy-2-naphthoic acids: crystal structures, theoretical computations, and permeation studies, *Cryst. Growth Des.*, 2020, **20**, 923–933.

41 C. C. P. Da Silva, C. C. de Melo, M. S. Souza, L. F. Diniz, R. L. Carneiro and J. Ellena, 5-Fluorocytosine/5-fluorouracil drug-drug cocrystal: a new development route based on mechanochemical synthesis, *J. Pharm. Innov.*, 2018, **14**, 50–56.

42 M. Mohana, P. T. Muthiah and C. D. McMillen, Supramolecular hydrogen-bonding patterns in 1:1 cocrystals of 5-fluorouracil with 4-methylbenzoic acid and 3-nitrobenzoic acid, *Acta Crystallogr., Sect. C: Struct. Chem.*, 2017, **73**, 259–263.

43 A. J. E. Duncan, R. L. Dudovitz, S. J. Dudovitz, J. Stojaković, S. V. S. Mariappan and L. R. MacGillivray, Quantitative and regiocontrolled cross-photocycloaddition of the anticancer drug 5-fluorouracil achieved in a cocrystal, *Chem. Commun.*, 2016, **52**, 13109–13111.

44 D. Voet and A. Rich, Structure of an intermolecular complex between cytosine and 5-fluorouracil, *J. Am. Chem. Soc.*, 1969, **91**, 3069–3075.

45 S. H. Kim and A. Rich, A non-complementary hydrogen-bonded complex containing 5-fluorouracil and 1-methylcytosine, *J. Mol. Biol.*, 1969, **42**, 87–95.

46 S. Zaitu, Y. Miwa and T. Taga, A 2:1 molecular complex of theophylline and 5-fluorouracil as the monohydrate, *Acta Crystallogr., Sect. C: Cryst. Struct. Commun.*, 1995, **51**, 1857–1859.

47 N. I. Nadzri, N. H. Sabri, V. S. Lee and S. N. A. Halim, 5-Fluorouracil co-crystals and their potential anti-cancer activities calculated by molecular docking studies, *J. Chem. Crystallogr.*, 2016, **46**, 144–154.

48 A. Delori, M. D. Eddleston and W. Jones, Cocrystals of 5-fluorouracil, *CrystEngComm*, 2013, **15**, 73–77.

49 U. P. Singh, S. Kashyap, H. J. Singh, B. K. Mishra, P. Roy and A. Chakraborty, Effect of adenosine on the supramolecular architecture and activity of 5-fluorouracil, *J. Mol. Struct.*, 2012, **1014**, 47–56.

50 A. K. Khan, R. Rashid, N. Fatima, S. Mahmood, S. Mir, S. Khan, N. Jabeen and G. Murtaza, Pharmacological activities of protocatechuic acid, *Acta Pol. Pharm.*, 2015, **72**, 643–650.

51 Z. Sroka and W. Cisowski, Hydrogen peroxide scavenging, antioxidant and anti-radical activity of some phenolic acids, *Food Chem. Toxicol.*, 2003, **41**, 753–758.

52 F. Abedi, B. M. Razavi and H. Hosseinzadeh, A review on gentisic acid as a plant derived phenolic acid and metabolite of aspirin: comprehensive pharmacology, toxicology, and some pharmaceutical aspects, *Phytother. Res.*, 2019, 1–13.

53 H. Yuasa, J. Gu, Y. Hayashi and J. Watanabe, First-pass metabolism of 5-fluorouracil in rats, *J. Pharm. Pharmacol.*, 1998, **50**, 1019–1025.

